Real-time Doppler-assisted tomography of microstructured fibers by side-scattering.

Stefani, Alessio ; Frosz, Michael H.; Euser, Tijmen G.; Wong, Gordon K. L.; Russell, Philip St J.

Link back to DTU Orbit

Real-time Doppler-assisted tomography of microstructured fibers by side-scattering

Alessio Stefani,[1,*] Michael H. Frosz,[1] Tijmen G. Euser,[1] Gordon K. L. Wong,[1] and Philip St.J. Russell[1,2]

[1]*Max Planck Institute for the Science of Light, Guenther-Scharowsky Str. 1, 91058 Erlangen, Germany*
[2]*Department of Physics, University of Erlangen-Nuremberg, 91058 Erlangen, Germany*
[*]*alessio.stefani@mpl.mpg.de*

Abstract: We introduce the concept of Doppler-assisted tomography (DAT) and show that it can be applied successfully to non-invasive imaging of the internal microstructure of a photonic crystal fiber. The fiber is spun at ~10 Hz around its axis and laterally illuminated with a laser beam. Monitoring the time-dependent Doppler shift of the light scattered by the hollow channels permits the azimuthal angle and radial position of individual channels to be measured. An inverse Radon transform is used to construct an image of the microstructure from the frequency-modulated scattered signal. We also show that DAT can image sub-wavelength features and monitor the structure along a tapered fiber, which is not possible using other techniques without cutting up the taper into several short pieces or filling it with index-matching oil. The non-destructive nature of DAT means that it could potentially be applied to image the fiber microstructure as it emerges from the drawing tower, or indeed to carry out tomography on any transparent microstructured cylindrical object.

References and links

1. P. St. J. Russell, "Photonic Crystal Fibers," Science **299**(5605), 358–362 (2003).
2. S. P. Stark, J. C. Travers, and P. St. J. Russell, "Extreme supercontinuum generation to the deep UV," Opt. Lett. **37**(5), 770–772 (2012).
3. J. M. Dudley and J. R. Taylor, *Optical Fiber Supercontinuum Generation* (Cambridge University Press, 2010), Chap. 7.
4. J. M. Dudley, G. Genty, and S. Coen, "Supercontinuum generation in photonic crystal fiber," Rev. Mod. Phys. **78**(4), 1135–1184 (2006).
5. A. D. Yablon, "Multi-Wavelength Optical Fiber Refractive Index Profiling by Spatially Resolved Fourier Transform Spectroscopy," J. Lightwave Technol. **28**(4), 360–364 (2010).
6. A. Barty, K. A. Nugent, D. Paganin, and A. Roberts, "Quantitative optical phase microscopy," Opt. Lett. **23**(11), 817–819 (1998).
7. J. B. Aniano, "System for determining birefringent axes in polarization-maintaining optical fiber," U.S. patent005317575A (May 31, 1994).
8. L. S. Watkins, "Scattering from side-illuminated clad glass fibers for determination of fiber parameters," J. Opt. Soc. Am. **64**(6), 767–772 (1974).
9. P.-E. Hansen and S. Burger, "Investigation of microstructured fiber geometries by scatterometry," Proc. SPIE **8789**, 87890R (2013).
10. L. Y. Zang, T. G. Euser, M. S. Kang, M. Scharrer, and P. St. J. Russell, "Structural analysis of photonic crystal fibers by side scattering of laser light," Opt. Lett. **36**(9), 1668–1670 (2011).
11. S. D. Lim, S.-G. Lee, K. Lee, and S. B. Lee, "Determination of Crystallographic Axes of Photonic Crystal Fiber by Transversal Scanning Method," Jpn. J. Appl. Phys. **49**(10), 102503 (2010).
12. A. D. Yablon, "Multifocus tomographic algorithm for measuring optically thick specimens," Opt. Lett. **38**(21), 4393–4396 (2013).
13. M. Jenkins and T. Gaylord, "3D Characterization of the Refractive-Index and Residual-Stress Distributions in Optical Fibers," in *Frontiers in Optics 2012/Laser Science XXVIII*, OSA Technical Digest (Optical Society of America, 2011), paper FMG4.

14. W. Gorski and W. Osten, "Tomographic imaging of photonic crystal fibers," Opt. Lett. **32**(14), 1977–1979 (2007).
15. A. Stefani, M. H. Frosz, T. G. Euser, G. K. L. Wong, and P. St. J. Russell, "*Doppler-Assisted Tomography of Photonic Crystal Fiber Structure by Side-Scattering*," in *Conference on Lasers and Electro-Optics, Technical Digest (CD) (Optical Society of America, 2014)*.
16. H. H. Barrett, "The Radon Transform and its Applications," in *Progress in Optics XXI*, E. Wolf ed. (North Holland, 1984).
17. A. G. Lindgren and P. A. Rattey, "The Inverse Discrete Radon Transform with Applications to Tomographic Imaging Using Projection Data," in *Advances in Electronics and Electron Physics 56*, C. Marton ed. (Academic Press, 1981).
18. C. M. Vest, "Formation of images from projections: Radon and Abel transforms," J. Opt. Soc. Am. **64**(9), 1215–1218 (1974).
19. *T. W. Haensch, Nobel Lecture (2005);* http://www.nobelprize.org/nobel_prizes/physics/laureates/2005/hansch-lecture.pdf.
20. A. Lange and M. P. Hentschel, "Direct Iterative Reconstruction of Computed Tomography Trajectories (DIRECTT)," in *Proceedings of DIR 2007 - International Symposium on Digital industrial Radiology and Computed Tomography,* Technical Digest (CD) (INSA-Lyon, 2007).
21. L. Zang, M. S. Kang, M. Kolesik, M. Scharrer, and P. St. J. Russell, "Dispersion of photonic Bloch modes in periodically twisted birefringent media," J. Opt. Soc. Am. B **27**(9), 1742–1750 (2010).
22. G. K. L. Wong, L. Zang, M. S. Kang, and P. St. J. Russell, "Measurement of group-velocity dispersion of Bloch modes in photonic-crystal-fiber rocking filters," Opt. Lett. **35**(23), 3982–3984 (2010).
23. G. K. L. Wong, M. S. Kang, H. W. Lee, F. Biancalana, C. Conti, T. Weiss, and P. St. J. Russell, "Excitation of Orbital Angular Momentum Resonances in Helically Twisted Photonic Crystal Fiber," Science **337**(6093), 446–449 (2012).
24. M. W. Zwierlein, J. R. Abo-Shaeer, A. Schirotzek, C. H. Schunck, and W. Ketterle, "Vortices and superfluidity in a strongly interacting Fermi gas," Nature **435**(7045), 1047–1051 (2005).

1. Introduction

The optical properties of photonic crystal fiber (PCF) are intimately linked to its microstructure [1–4]. To achieve a desired performance, the PCF microstructure must be optimized by adjusting drawing parameters such as temperature, air-hole pressure, drawing tension and drawing speed. While currently available optical index profiling methods provide useful real-time feedback during the drawing of standard step-index fibers, these methods require a low refractive index contrast and cannot be transferred to non-invasive or non-destructive imaging of PCF [5–8].

Currently the PCF microstructure is monitored by manually collecting a sample from the drawing tower and cleaving it for examination in an optical or scanning electron microscope (SEM). If the drawing parameters need to be adjusted, a new sample is taken after some time to let the changes take effect. This is repeated iteratively until the desired microstructure is achieved. This procedure has the drawbacks that the optimization process takes at least half an hour, wastes a lot of fiber (the fiber drawing process cannot be stopped) and is destructive, making it impossible to monitor the quality of the inner PCF structure during collection of a long length of fiber. Also, manual collection of fiber samples is not feasible at the high drawing speeds required for certain fiber types.

All these problems could be avoided if a non-invasive technique could be found for real-time monitoring of the fiber microstructure during the draw. The drawing parameters could then be rapidly optimized for a desired microstructure without cutting the fiber, and an automated control system could be designed to keep the microstructure constant, or to vary it slowly or periodically over long fiber lengths.

If the hollow channels are filled with a fluid of index close to that of silica (so as to reduce multiple scattering), the microstructure in PCF can be measured by side-scattering. Two main approaches have been used. In the first the pattern created by scattering of a laser beam was used to derive information about the pitch [9] and the orientation [10,11] of the microstructure, without actually imaging it. In the second, a set of index profiles taken at different fiber orientations was used to tomographically reconstruct the structure [12–14]. This required several hours of data-processing per image [12], making real-time monitoring impossible. It is clear that neither of these approaches is suitable for use in fiber drawing.

Here we report a novel non-destructive technique that enables rapid reconstruction, from side-scattered light, of the main features of the internal microstructure of PCFs [15]. The approach combines detection of the Doppler shift of light scattered by a rotating PCF with the back-projection reconstruction method commonly used in medical imaging systems such as MRI [16]. In this proof-of-principle study the fiber itself is rotated, keeping the illumination and detection angles fixed. Each hollow channel in the fiber produces a Doppler shift that depends on its radial and azimuthal position within the PCF. From the frequency spectrum, the fiber structure can be reconstructed by back-projecting the data using an inverse Radon transform [16–18]. Since an entire data set is acquired after only one rotation and can be processed within less than a second, it is possible to obtain real-time information about the fiber structure. We call this technique Doppler-assisted tomography (DAT).

In general, frequency-based detection schemes allow very accurate measurements that are robust against amplitude fluctuations, as already pointed out by Hänsch [19]. We demonstrate that DAT allows non-destructive imaging of the microstructure of simple PCFs, as well as imaging the internal microstructure profile along tapered PCF. The results also show that sub-wavelength holes (below 90 nm in diameter at a wavelength of 633 nm) can be successfully detected.
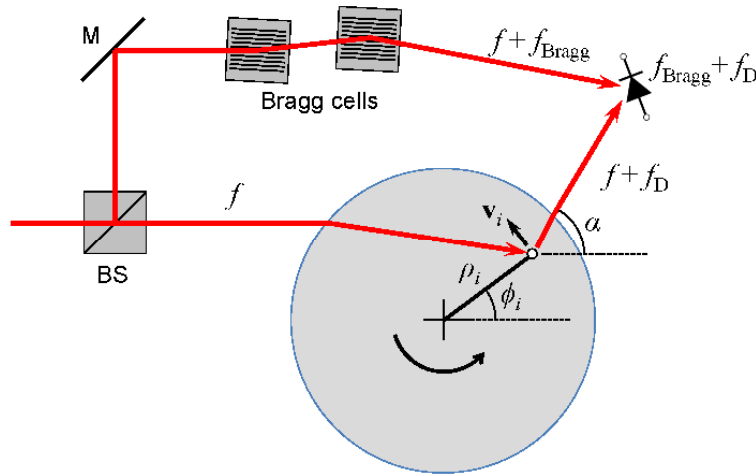

Fig. 1. Schematic of the DAT set-up at $t = 0$ (not to scale). One part of the laser beam is incident on the rotating fibre, the other being frequency shifted at a pair of Bragg cells. The Doppler-shifted scattered light (f_D ~1 kHz is a typical value at f_{rot} ~300 rpm) is combined with the frequency-shifted light and the beat-note detected at a square-law detector.

2. Working principle and set-up

A schematic of the experimental set-up is shown in Fig. 1. Light from an incident laser beam is scattered by the fiber, which spins at $f_{rot} = \Omega/2\pi$. Light scattered at an angle α to the incoming beam is mixed with a fixed-frequency reference beam, and the resulting intensity beat-note detected by a photodiode. Two Bragg cells are used to frequency-shift the reference beam, as to discriminate between positive and negative Doppler-shifts. For small frequency shifts, the Doppler shift may be written in general as $f_D = (\mathbf{n}_S - \mathbf{n}_I) \cdot \mathbf{v} / \lambda$ where $\mathbf{n}$ is the refractive index vector of the light, I and S refer to the incident and scattered signals, $\mathbf{v}$ is the velocity of the scatterer and λ the vacuum wavelength. Applying this expression to the set-up in Fig. 1, the Doppler-shift for the i-th scatterer turns out to be a sinusoidal function of time:

$$f_D(t) = \frac{\Omega \rho_i \, n}{\lambda} \cos\left(\Omega t + \phi_i - \frac{\alpha}{2}\right) \sin\frac{\alpha}{2} \qquad (1)$$

where α is the angle between the incident and scattered wave vectors, c is the speed of light in vacuum, ρ_i and ϕ_i are the radial and angular positions of the i-th feature at time $t = 0$, and n is the refractive index of the glass.
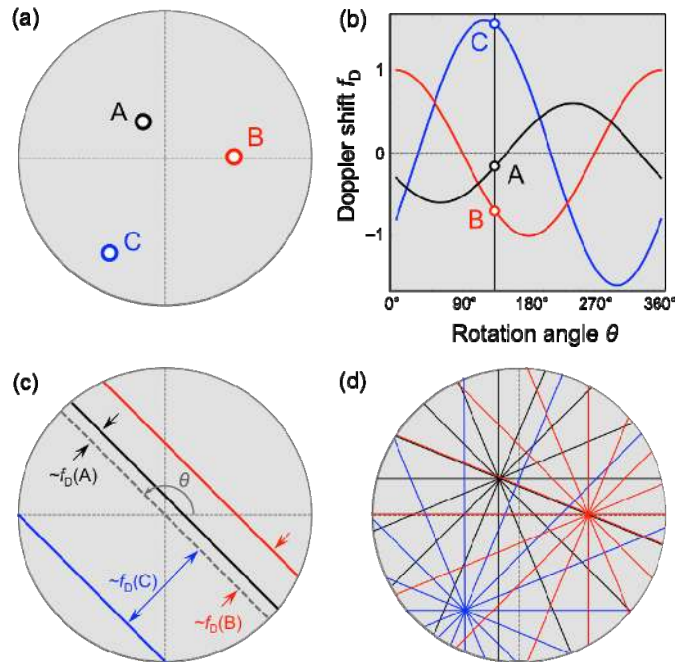

Fig. 2. Illustration of the working principle of DAT. (a) Sample structure with three holes. (b) Frequency shift f_D versus rotation angle assuming single scattering (follows Eq. (1)). The vertical black line indicates the rotation angle θ analyzed further in Fig. 2(c). (c) Possible locations of each hole lie on straight lines, sloping at angle θ, spaced from the origin a distance proportional to f_D. (d) Combination of several snap-shots at different angles yields the positions of the scatterers.

In the experiment the intensity of the scattered signal is recorded as a function of time. A time-windowed Fourier transform is then used to recover a time-frequency plot that corresponds to Eq. (1).

To recover the position of the scatterers, a procedure similar to the inverse Radon transform [17,18], commonly used in tomography, was used. The principle is illustrated in Fig. 2 for the simple case of three scatterers. At each angle on the frequency-angle spectrogram, the possible hole positions that could have produced the signal lie on straight lines, tilted by the rotation angle and at a distance from the center of rotation that is proportional to the frequency shift (Fig. 2(c)). The positions of these lines are associated experimentally with peaks in the measured spectrum at a given angle, each of which is associated with a scatterer – see Fig. 3(c,g). When this process is repeated for a series of different angles, the positions of the scatterers are given by the intersections of all the different lines (Fig. 2(d)).

In conventional tomography, the transverse phase or intensity profile of a beam transmitted through a sample is measured at a number of different orientations. These are then combined to obtain a trace of transverse position versus rotation angle, which is then inverse Radon-transformed to obtain the position of features within the cross-section. The DAT technique differs in one important respect: instead of measuring the entire transverse profile, Doppler spectra are obtained for each rotation angle. This has the major advantage that all the spatial information is encoded in the frequency domain, which means that a single point detector can be used. An additional advantage is that, unlike conventional methods, the spatial

resolution is not limited by the imaging resolution of the detection system. Furthermore, data over the entire range of angular orientations can be measured in a single rotation period, greatly reducing the measurement time.

In the experiments a HeNe laser emitting 12 mW at a wavelength of 632.8 nm was used. The rotation speed was set to ~10 Hz and the scattering angle α was 90°. The PCFs studied had holes distant between 1 and ~50 μm from the axis of rotation, resulting in frequency shifts ranging from ~100 Hz to 1 kHz. By driving the two Bragg cells at slightly different frequencies, the reference signal was shifted by 10 kHz. As a result, the measured signal contained frequency components of 10 kHz ± 2 kHz that could easily be detected using a photodiode and an oscilloscope. The scattered signal was collected using the tip of a single mode fiber, and mixed with the reference signal (also fiber-delivered) at a 99:1 coupler. A polarization controller was used in the reference arm to allow the intensity of the beat signal to be optimized. The whole set-up, including acquisition, signal processing and translation stages, was computer controlled.

The precision with which the position of a scatterer can be measured depends on the frequency resolution of the time-windowed Fourier transform (or any other transform used to convert the photodetector signal into a time-frequency trace) and on the number of time windows used. In the experiments a resolution of ~10 Hz in the Doppler frequency shifts was typically used, corresponding to a spatial resolution of 100 nm. The time windows were typically 1/20th of the rotation period and consecutive windows had an overlap of ~80%, yielding a total of 70 to 200 angular projections. So as to ensure coverage of a full period, data was typically acquired for 1.2 rotation periods and the total measurement time was ~100 ms. Signal processing took around 500 ms, so the total reconstruction time was below 1 second.

Resolving the position of a hole close to the axis might become an issue if it produces a maximum Doppler shift that is close to the frequency resolution of the system. For the experimental parameters used, however, none of the holes produce a Doppler shift that is less than 10 times larger than the minimum detectable frequency shift.

To avoid distortions in the frequency-angle traces it was important to perfectly align the fiber perpendicular to the illumination-detection plane. This proved to be very difficult, so a calibration scheme was implemented: the incident beam was displaced sideways so that it was reflected from the outer surface of the fiber. Small residual movements of the fiber, caused by misalignment, could then be accurately measured and the information used afterwards to correct the data in the actual measurements.

3. One-shot DAT reconstructions

In order to test the technique in structures with high index contrast, fibers with a small number of holes were investigated. The first of these had three asymmetrically placed off-center holes (Fig. 3(a)). The corresponding windowed fast Fourier transform (FFT) shows several clear curves (Fig. 3(b)), each corresponding to a single scattering center. This spectrogram was used to reconstruct the fiber profile (Fig. 3(d)) using the inverse Radon transform. The DAT reconstructions are in good agreement with the SEMs. In addition to the three large holes, the DAT image uncovered a fourth feature that was invisible under the optical microscope.
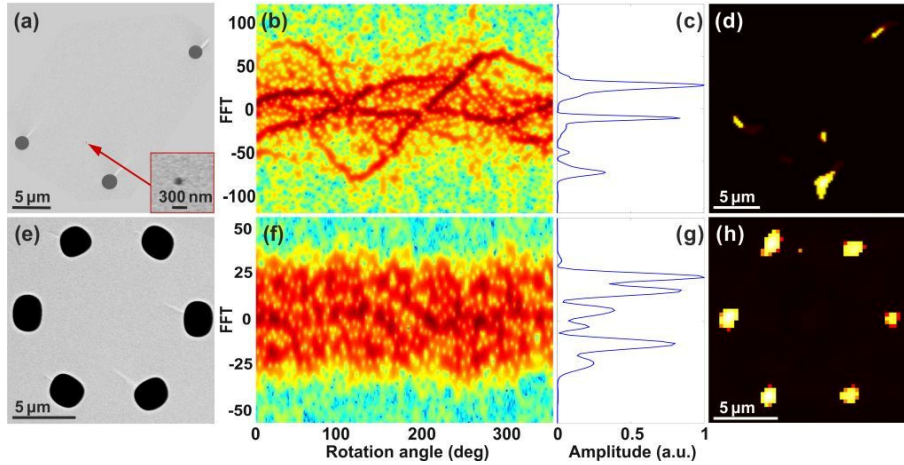
Fig. 3. (a,e) Scanning electron micrographs (SEMs) of simple structures. (b,f) Apertured fast Fourier transforms (FFTs). The y-axis shows the frequency shifts normalized to the rotation frequency. (c,g) Examples of the spectra of the time-apertured FFTs at one rotation angle. (d,h) DAT reconstructions of (a) and (e) using the inverse Radon transform.

A high-resolution SEM confirmed the existence of a ~150-nm-wide channel at the indicated position (such unwanted defects are caused by uncollapsed air-holes in the fiber preform and often cannot be detected in an optical microscope).
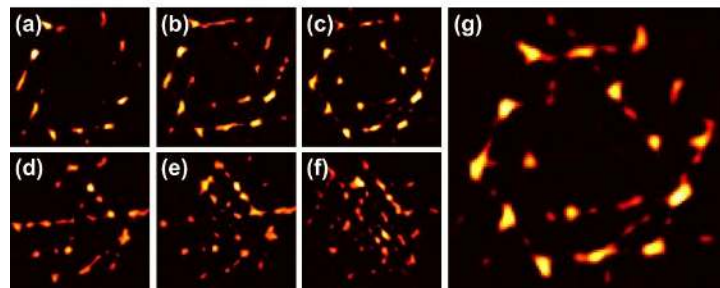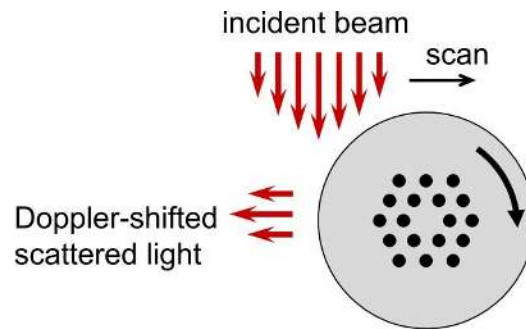

Fig. 4. Schematic of the principle behind reduction of multiple scattering. The illuminating beam is scanned across the structure. (a) to (f) Reconstructions made as more and more of the structure is illuminated by the beam. The scan distance between each measurement was ~4 μm and the laser beam width was ~20 μm FWHM. (g) Image obtained by summing reconstructions (a) to (e).

The second was a fiber with six hexagonally-placed air-holes of diameter ~2.5 μm and spacing 6.7 μm (Figs. 3(e-h)). This time the scattering data (Fig. 3(f)) was significantly disturbed by multiple scattering, making it impossible to distinguish distinct individual curves

on the spectrograms. Nevertheless, the inverse Radon transform proved robust enough to allow retrieval of the positions of the six holes (Fig. 3(h)).

4. Reducing the effects of multiple scattering

When attempting to measure a PCF with two rings of air-holes positioned hexagonally, multiple scattering and interference prevented clear reconstruction of the structure. To reduce the severity of this problem, a narrower illuminating beam, scanned linearly across the fiber, was used, the idea being to illuminate only one strip at the time. In this way fewer features are illuminated simultaneously, reducing the total degree of multiple scattering. Moreover, the range of Doppler frequency shifts is reduced, allowing other components to be filtered out. Figure 4 shows the images produced when a beam is scanned across the structure. At first only the outer ring is visible, and as the beam moves towards the fiber center the inner ring of holes appears in the reconstructed image. Finally, when almost the whole structure is illuminated, the structure can no longer be clearly distinguished. Summing the various reconstructions, however, allows the fiber structure to be nicely reconstructed. To obtain the summed reconstruction, each reconstruction image was normalized to 1 and the different images were added pixel by pixel. Given the properties of the inverse Radon transform, a full scan through the structure is not necessary. In fact, a partial sinusoidal component in the spectrogram is enough to reconstruct the position of a scatterer. This can also be a drawback, because small artifacts in the traces can turn into non-existent features in the reconstruction.
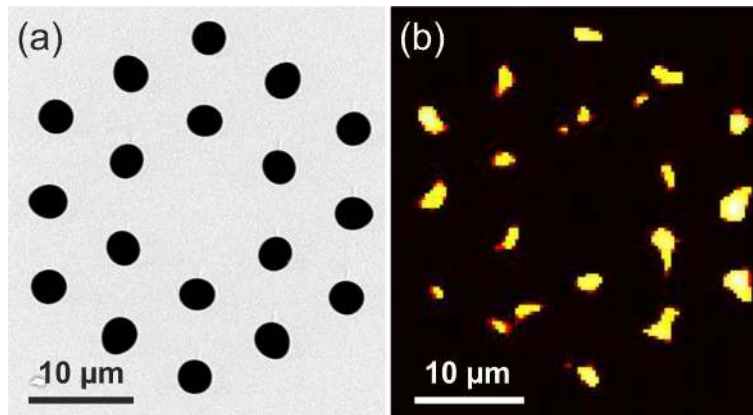

Fig. 5. (a) SEM of a PCF with two rings of air-holes. (b) DAT reconstruction obtained by scanning across the structure and by summing the different contributions; 23 different reconstructions were summed.

To implement this approach, the illuminating beam diameter was reduced to ~20 µm using a lens of focal length 30 mm, and then scanned across the fiber. The DAT reconstruction of a structure with 18 channels arranged in two hexagonal rings is shown in Fig. 5. It was generated by summing 23 images obtained by scanning a distance of ~50 µm across the fiber.

Although DAT image Fig. 5(b) is distorted by residual multiple scattering, this could also be related to the hollow channels not being perfectly circular, which would introduce an angular dependence in the scattered signal strength, resulting in frequency-angle traces that are not purely sinusoidal (e.g. Figure 3(b)). Thus, whereas very small circular holes will be perfectly reproduced by the inverse Radon transform, the reconstruction of a non-circular hole will be smeared out into two or more points. This could perhaps be used to obtain information about the shape of the hollow channels.
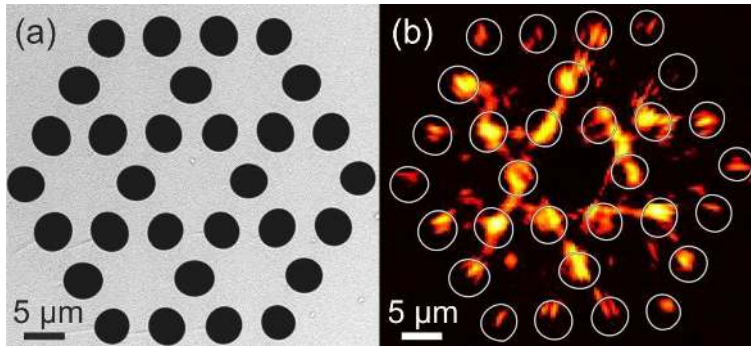
Fig. 6. (a) SEM of a PCF with three rings. (b) DAT reconstruction obtained by scanning across the structure and by summing 17 different reconstructions. The reconstruction is plotted with the contours of the actual fiber structure overlaid.

Having demonstrated the effectiveness of lateral scanning to reduce multiple scattering, we measured the more complicated structure in Fig. 6(a). The DAT reconstruction in Fig. 6(b) was made by adding together 17 images; for comparison the contours of the actual structure are overlaid. Although the image is not perfect, it is possible to identify the features of this particular structure well enough to monitor its pitch if the DAT system were implemented in a fiber drawing tower.
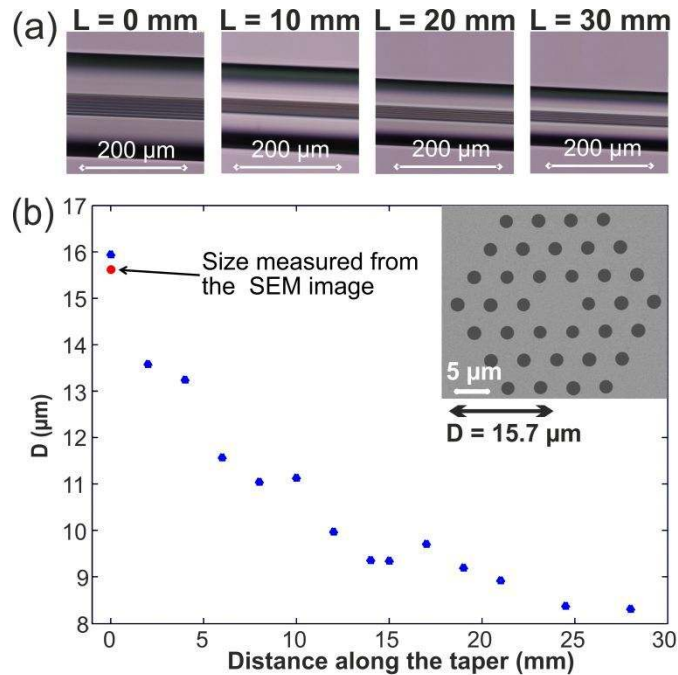

Fig. 7. Measurements of a fiber taper. (a) Optical side-images of the PCF. (b) Diameter of the internal structure reconstructed by DAT, plotted against position along the taper. Inset: SEM of the fibre structure at the beginning of the taper.

To illustrate the potential of DAT, and the useful information that can be obtained even without reconstructing all the details of the microstructure, the overall size of the microstructured region along a tapered PCF sample was measured (the diameter-dependence of the zero dispersion wavelength has been used to enhance supercontinuum generation [2–4]). Figure 7(a) shows optical micrographs taken through the side at four positions along the taper. In the DAT experiment no attempt was made to reduce multiple scattering, since we

were interested solely in measuring the distance between the outer corners of the microstructured region. This was done by directly monitoring (using a 10 dB threshold) the maximum Doppler shift, i.e., without applying the inverse Radon transform. The reconstructed corner-to-corner dimensions of the microstructure along the taper are in excellent agreement with those measured in the SEM. This is the first time the microstructure along a tapered PCF has been measured non-destructively.

5. Identifying sub-wavelength features

DAT may be used to detect any moving object that scatters light, and will also work for objects much smaller than the optical wavelength. It has already been shown in Fig. 3(d) that a feature ~150 nm could be detected. To further explore this, three samples of two-ring PCFs with air-hole diameters ranging from 40 nm to 1 μm were prepared by varying the pressure during fiber drawing. SEMs of the resulting structures are shown in Fig. 8(a-c), and DAT reconstructions of each, made using the lateral scanning technique described in Section 4, are shown in Fig. 8(d-f). In all cases the holes could be clearly identified, even when they were as small as 90 nm and the scattered signal quite weak. In the third case, no open holes could be seen in the optical microscope, whereas DAT detected the presence of one. Subsequent SEM imaging showed that a ~160 nm channel was still open in the fiber. Finding the position of such a small and solitary hole is challenging even with SEM and would almost certainly have been overlooked if DAT had not been used.
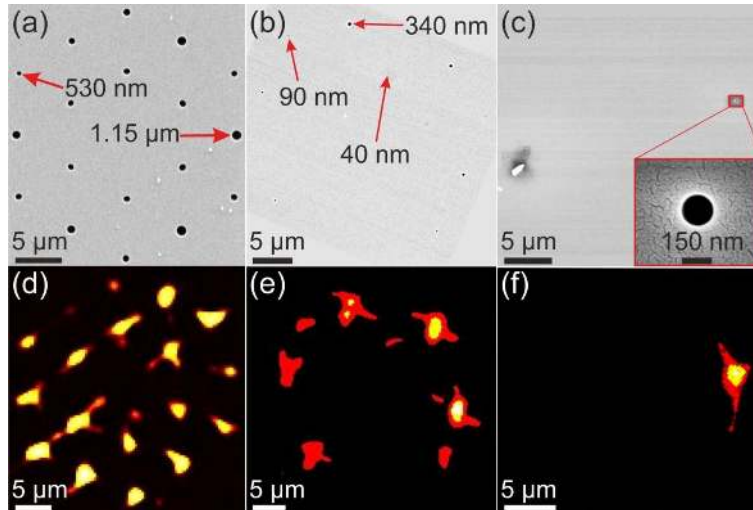

Fig. 8. (a-c) SEMs of the PCF fabricated for studying the identification of tiny holes. The hole diameter ranges are: (a) 1.15 μm to 530 nm, (b) 340 nm to 40 nm (c) 160 nm. (d-f) DAT reconstructions of the fibers showed in (a-c).

6. Discussion and conclusions

The technique as currently implemented has some limitations. As mentioned in Section 4, the hollow channels in PCF are not point-scatterers but have finite size and are often not perfectly circular. Both these factors lead to Doppler-shift traces that deviate from the purely sinusoidal form in Eq. (1). This means that the lines used to locate the positions of the holes (Fig. 2(c)) do not intersect exactly at one point, i.e., the reconstruction is blurred. Another type of distortion occurs because of refraction at the curved outer surface of the fiber. This means that the optical path lengthens and shortens (compared to its length in the absence of refraction) periodically as the fiber rotates, causing the Doppler shift again to deviate from Eq. (1). This effect is however important only if a hole is positioned close to the outer edge of the fiber, and is insignificant in all the cases discussed in this paper. Although these effects distort the

reconstruction, they create systematic features in the frequency-angle spectra that, if understood, could potentially be used to improve the imaging. The use of multiple detectors may also provide a means of enhancing the reconstruction.

As we have shown, lateral scanning of the incident beam reduces multiple scattering effects and could be further optimized. The unavoidable trade-off between spot-size and Rayleigh length, however, limits this technique to structures where the density of scatterers is not too high. The DAT reconstruction could be further improved using an iterative algorithm [20]. This would reduce the noise and sharpen the edges of the reconstructed features. Such an algorithm would make use of an analytical mask that matches the desired structure, allowing for free parameters such as pitch and the presence or absence of air-holes, so as to simplify the reconstruction problem.

In conclusion, DAT allows the basic dimensions of the internal microstructure of a PCF to be monitored non-destructively. Based on the measurement of a frequency shift and not an amplitude, it is intrinsically easier to implement and produces an image within less than a second – much faster than other non-invasive techniques. DAT is very good at identifying features much smaller than the optical wavelength that are not visible using conventional optical methods.

DAT could be used to monitor the structure of any microstructured strand of transparent material. The opportunity not only to reconstruct the structural features but also to determine the structural orientation could be useful for monitoring twisted fibers and rocking filters [21–23]. Moreover, DAT has the potential to be also used for the investigation and imaging of complex systems, as for example to detect vortices in a superfluid Fermi gas [24], where sub-wavelength air channels are the fingerprint of superfluidity.

In future work, as well as further improving the technique (for example investigating in more detail the imaging of finite sized non-circular features), we plan to implement the set-up on a fiber drawing tower by arranging the illumination-detection system to spin around the fiber.